


RESEARCH ARTICLE

Hydrophilic cryogels as potential 3D cell culture materials: Synthesis and characterization of 2-(methacrylamido) glucopyranose-based polymer scaffolds

Florian Behrendt^{1,2} | David Pretzel^{1,2,3} | Zoltán Cseresnyés⁴ |
Maximilian Kleinsteuber^{1,2} | Thomas Wloka^{1,2} | Lukáš Radosa⁵ |
Marc Thilo Figge^{4,6} | Michael Gottschaldt^{1,2} | Axel Brakhage^{5,6} |
Ulrich S. Schubert^{1,2,3} 

¹Laboratory of Organic and Macromolecular Chemistry (IOMC), Friedrich Schiller University Jena, Jena, Germany

²Jena Center for Soft Matter (JCSM), Friedrich Schiller University Jena, Jena, Germany

³Abbe Center of Photonics (ACP), Friedrich Schiller University Jena, Jena, Germany

⁴Applied Systems Biology, Leibniz Institute for Natural Product Research and Infection Biology, Hans Knöll Institute (HKI), Jena, Germany

⁵Molecular and Applied Microbiology, Leibniz Institute for Natural Product Research and Infection Biology, Hans Knöll Institute (HKI), Jena, Germany

⁶Institute of Microbiology, Faculty of Biological Sciences, Friedrich Schiller University Jena, Jena, Germany

Correspondence

Ulrich S. Schubert, Laboratory of Organic and Macromolecular Chemistry (IOMC), Friedrich Schiller University Jena, Humboldtstraße 10, 07743 Jena, Germany. Email: ulrich.schubert@uni-jena.de

Funding information

Deutsche Forschungsgemeinschaft, Grant/Award Numbers: 390713860, 316213987, SCHU 1229/25-1, LI 916/19-1, GO 1100/4-1

Abstract

Cell cultures are important techniques to investigate cellular processes in a simplified manner. The most commonly applied 2D models do not simulate most of the in vivo conditions whereas cryogels as promising 3D cell culture materials are able to provide both a structured microenvironment and tailored surface properties, similar to the natural extracellular matrix (ECM). Herein, we present the synthesis and characterization of hydrophilic cryogels with different 2-(methacrylamido) glucopyranose amounts followed by 3D cell culture experiments with L929 cells. Selected samples are additionally functionalized with fibronectin-FITC for improved cellular adhesion. The incorporation of different 2-(methacrylamido) glucopyranose amounts into the cryogels is demonstrated by Fourier-transform IR (FTIR) and solid-state NMR (ssNMR). The gels are able to withstand harsh autoclaving conditions as shown by thermogravimetric analysis (TGA) and ssNMR measurements. Pore size measurements by automated scanning electron microscopy (SEM) image analysis reveal similar pore sizes among the entire cryogel series. Confocal laser scanning microscopy (CLSM) images suggest the presence of healthy cells due to the absence of morphological abnormalities among the entire cryogel series. L929 cells settled deeper into the cryogels with increasing MAG content. With additional fibronectin functionalization, the cells are retained much stronger and stay in the upper gel layers.

KEYWORDS

2-(methacrylamido) glucopyranose, 3D cell culture, hydrophilic cryogels, poly(2-ethyl-2-oxazoline) diacrylates

This is an open access article under the terms of the [Creative Commons Attribution-NonCommercial](https://creativecommons.org/licenses/by-nc/4.0/) License, which permits use, distribution and reproduction in any medium, provided the original work is properly cited and is not used for commercial purposes.

© 2023 The Authors. *Journal of Polymer Science* published by Wiley Periodicals LLC.

1 | INTRODUCTION

In vitro culturing of cells represents an important research tool in cell biology and biochemistry for the investigation of cellular proliferation, differentiation, metabolism as well as other cellular processes¹ and plays a key role in drug discovery, cancer, and stem cell research.² Most commonly, 2D culture methods, for example, micro-well plates, tissue culture flasks, or petri dishes are applied which are advantageous due to their practicability, low cost, and robustness. Nevertheless, in vivo conditions mostly of 3D character are insufficiently reproduced due to the absence of a structured microenvironment, which leads to possible misrepresentations of the resulting findings. For instance, the shape and proliferation of cells as well as their gene and protein expression profile strongly rely on the culture conditions.^{3,4} Adherent cells such as fibroblast cells from connective tissue are usually flat and elongated when cultured under 2D conditions, whereas 3D models enable to preserve the natural shape of cells and their growth as 3D aggregates resulting in a larger number of cell-to-cell interactions.^{3,4} Furthermore, levels for protein and gene expression of cells cultured using 3D techniques were found to be similar to in vivo conditions.^{3–5} To allow for the most representative and reliable outcomes, the applied techniques need to be able to mimic the natural extracellular matrix (ECM) conditions as closely as possible. The natural ECM consists of collagen and elastic fibers within a hydrated gel composed of glycosaminoglycans, proteoglycans, and glycoproteins.⁶ Apart from scaffold-free 3D techniques, such as hanging drop microplates, magnetic levitation, and spheroid microplates, scaffold-based 3D models offer the possibility to provide a structured surrounding architecture for cellular growth, similar to the natural ECM. Besides hydrophilic glass fibers and organoids as 3D scaffolds, a wide range of hydrogels have been applied as 3D culture materials based on synthetic polymers like poly(ethylene glycol),^{7–10} poly(vinyl alcohol),^{7,11} poly(caprolactone),^{9,12} or poly(lactic acid-co-glycolic acid).^{10,13} Besides natural polymers like polysaccharides (chitosan, alginate, dextran) or proteins (gelatin, collagen, fibrin), synthetic polymers offer tailored chemical and physical properties, for example, an improved mechanical stability. Limited bioactivity can be overcome by the attachment of bioactive molecules as, for example, fibronectin which contains the cell-binding arginyl-glycidyl-aspartate motif (RGD). Contrary to hydrogels, cryogels represent a class of macroporous polymeric scaffolds that are ideal for serving as 3D cell culture materials providing an enlarged surface for multiple cell growth, an enhanced cell-to-cell contact support, and act as artificial ECM mimics.¹⁴ Cryogels

consist of a sponge-like architecture due to the intrinsic pore structure of interconnected macropores. These cavities and channels allow the transport of substances like nutrients and the migration of microorganisms and eukaryotic cells through the material in case of sufficient pore sizes.^{15,16} Furthermore, the material properties of cryogels are adjustable depending on the desired applications and can be precisely tailor made. For instance, to introduce certain surface functionalities, appropriate building blocks can be chosen for cryogel synthesis. Mechanical properties such as stiffness and hardness can also be adjusted in the same fashion, mainly by the choice of the cross-linking unit. Besides the use in the cryopreservation of cells,^{17–22} there are lots of examples of cryogels used for cell culture applications. A variety of synthetic polymers like poly(acrylonitrile),²³ poly(*N*-isopropylacrylamide),^{23,24} poly(acrylamide),²³ poly(vinyl alcohol),²⁵ poly(2-hydroxypropylmethacrylamide),²⁶ poly(2-hydroxyethyl methacrylate) (HEMA),^{27–29} or poly(ethylene glycol)^{30–32} have been used for cryogel preparation separately or in combination with biopolymers like dextran,^{27,28} gelatin,^{24,29,32,33} heparin,³⁰ alginate,³³ or hyaluronan.¹⁷ Since highly hydrophilic materials are better mimics of aqueous in vivo environments,¹ cryogels with an increasing amount of the water-binding sugar-based building block 2-(methacrylamido) glucopyranose (MAG) were prepared in this study. So far, the monomer **MAG** was commonly applied for the preparation of affinity chromatography matrices for enzyme purification³⁴ or as a saccharide unit for the preparation of heparin-mimicking polymeric surfaces for cell culture studies^{35–42} but has never been used for the preparation of hydrophilic cryogels by now.

In this study, we report on the preparation and characterization of hydrophilic cryogels using *N,N'*-methylenebisacrylamide and tailor-made poly(oxazoline) diacrylates as cross-linkers with different portions of **MAG** as a sugar-containing monomer. Selected cryogel samples are additionally modified with fluorescein isothiocyanate-labeled fibronectin (fibronectin-FITC) to enhance cellular adhesion. Furthermore, we investigate the influence of the **MAG** amount and the fibronectin surface functionalization on the 3D culture of L929 cells, the cellular settlement into the materials, and their metabolic activity.

2 | RESULTS AND DISCUSSION

2.1 | Synthesis of cryogel building blocks 2-(methacrylamido) glucopyranose and poly(oxazoline) cross-linkers

For the preparation of cryogels, we utilized poly(2-ethyl-2-oxazoline) diacrylate cross-linkers **POx1** and **POx2**

which were already synthesized previously by cationic ring-opening polymerization in the presence of *trans*-1,4-dibromobut-2-ene (DBB) as a bi-functional initiator (Figure 1, panel (i)).⁴³

The hydrophilic sugar monomer 2-(methacrylamido) glucopyranose (**MAG**) was prepared according to a literature procedure (Figure 1, panel (ii)).⁴⁴ The crude product obtained from the reaction of methacryloyl chloride and glucosamine hydrochloride in the presence of potassium carbonate was purified by column chromatography (CH₂Cl₂:CH₃OH = 4:1). ¹H NMR and ¹³C NMR measurements of the isolated product fraction showed the presence of two anomeric forms of the product due to a

double set of signals (see Figures S1 and S2), which could be further confirmed by trapped ion mobility mass spectrometry (TIMS).

Herein, a separation of the two species was possible which were detected separately either as [M + Na⁺] or [2 M + Na⁺] species (Figure 2).

2.2 | Preparation of hydrophilic cryogels based on MAG

Hydrophilic cryogels were prepared in 5 mL polypropylene syringes as reaction molds via free radical

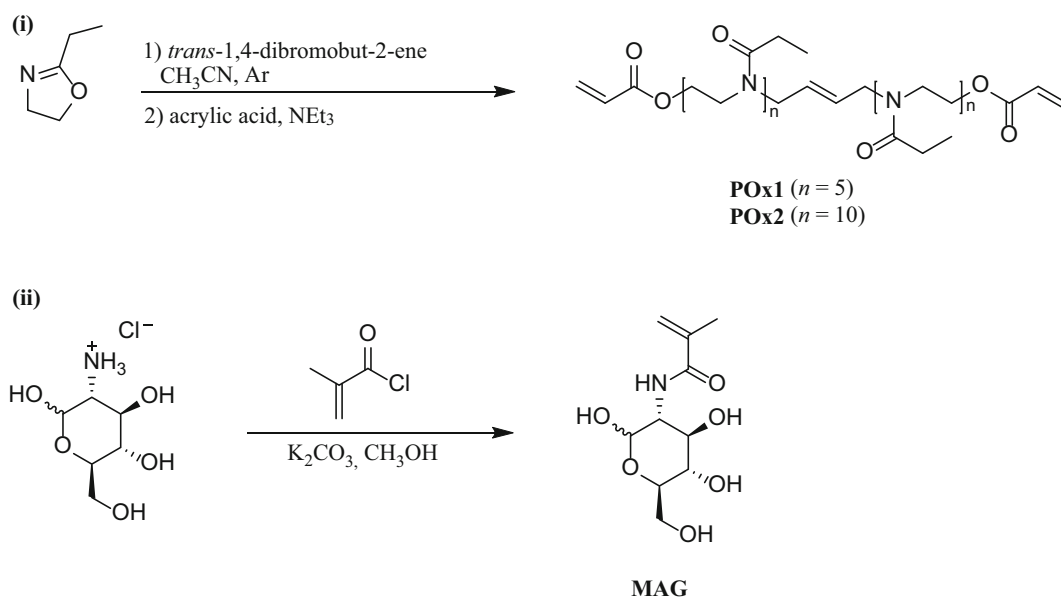


FIGURE 1 Panel (i): Schematic representation of the synthesis of poly(oxazoline) diacrylates **POx1** (DP10) and **POx2** (DP20) as macromolecular cross-linkers. Panel (ii): Schematic representation of the synthesis of 2-(methacrylamido) glucopyranose (**MAG**) as a hydrophilic carbohydrate building block.

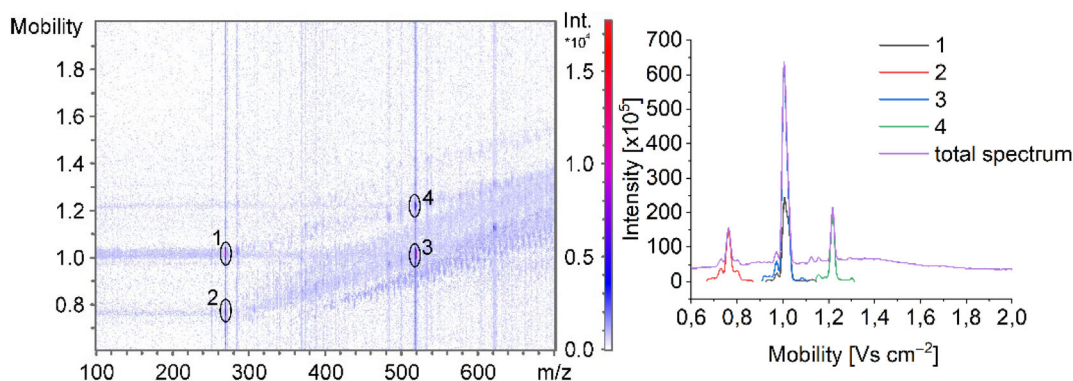
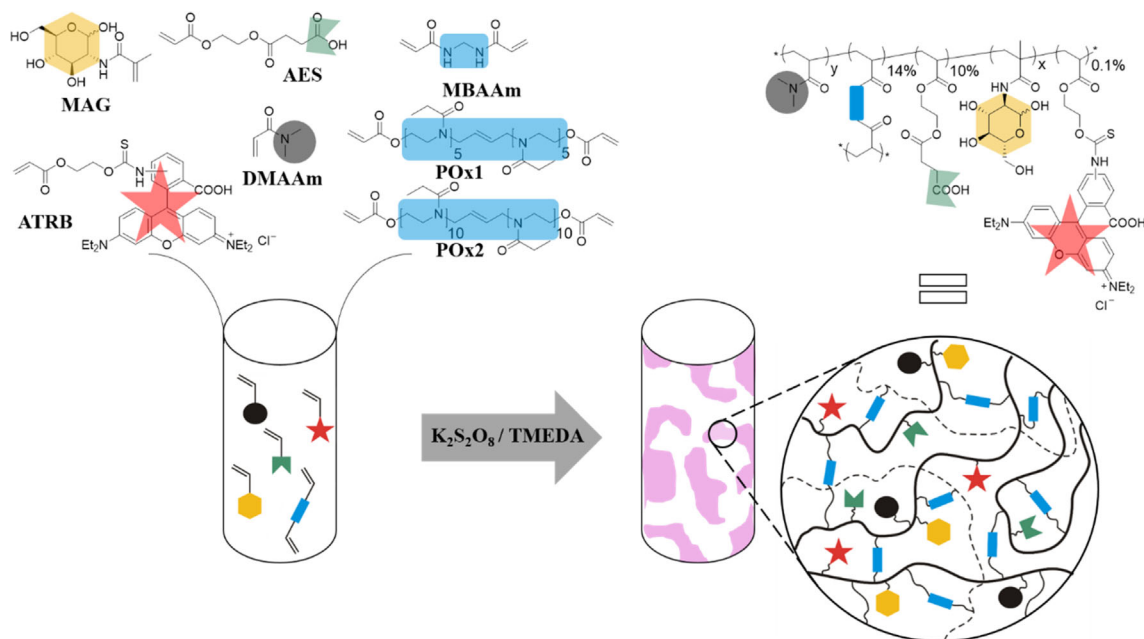


FIGURE 2 Overview of the trapped ion mobility mass spectrometry (TIMS) measurement results. Left: Heat map of 2-(methacrylamido) glucopyranose (**MAG**); m/z of selected peaks: 1 (270.0945, $M+Na^+$), 2 (270.0947, $M+Na^+$), 3 (517.1994, $2M+Na^+$), and 4 (517.1994, $2M+Na^+$). Right: Mobilogram visualizing the two different isomeric species.



SCHEME 1 Schematic representation of the preparation of glucosamine functionalized cryogels using different cross-linkers.

	MAG	DMAAm	AES	Cross-linker
CGBis-0, 26, 51, 76	0%/26%/51%/76%	76%/50%/25%/0%	10%	MBAAm 14%
CGPOx1-0, 26, 51, 76	0%/26%/51%/76%	76%/50%/25%/0%	10%	POx1 14%
CGPOx2-0, 26, 51, 76	0%/26%/51%/76%	76%/50%/25%/0%	10%	POx2 14%

TABLE 1 Overview of the library of cryogels and the different proportions (mol%) of each monomer in the feed solution.

Abbreviations: **AES**, mono(2-acryloyloxyethyl) succinate; **DMAAm**, *N,N*-dimethylacrylamide; **MAG**, 2-(methacrylamido) glucopyranose; **MBAAm**, *N,N'*-methylenebisacrylamide; **POx1**, poly(2-ethyl-2-oxazoline) diacrylate DP10; **POx2**, poly(2-ethyl-2-oxazoline) diacrylate DP20.

cross-linking polymerization at sub-zero temperatures (cryopolymerization). The radical formation was achieved by the use of $K_2S_2O_8$ and *N,N,N',N'*-tetramethylethylenediamine (TMEDA). 2-(Methacrylamido) glucopyranose (**MAG**) was selected as a carbohydrate-containing monomer to obtain specific surface functionalization and hydrophilic properties. Dimethylacrylamide (**DMAAm**) was chosen as a co-monomer to provide sufficient stability to the polymer network and was successively replaced with an increasing amount of **MAG** to incorporate different amounts of sugar into the polymer network. For potential post-polymerization modifications with e.g. biomolecules like proteins or peptides,

acryloyloxyethyl succinate (**AES**) was chosen as a functional co-monomer introducing carboxylic acid groups into the cryogels. The use of rhodamine B acrylate (**ATRB**) as a fluorescence label allowed the observation of the cryogel structure by FM and CLSM. A library of cryogels was prepared using various amounts of **MAG** (0%, 26%, 51%, 76%) and either a commercially available cross-linker *N,N'*-methylenebisacrylamide (**MBAAm**) or tailor-made poly(oxazoline) diacrylates (**POx1** and **POx2**) (Scheme 1, Table 1).

By the use of tailor-made poly(oxazoline) diacrylates as macromolecular cross-linkers, the influence of the cross-linkers on the gel properties as, for example, pore size was

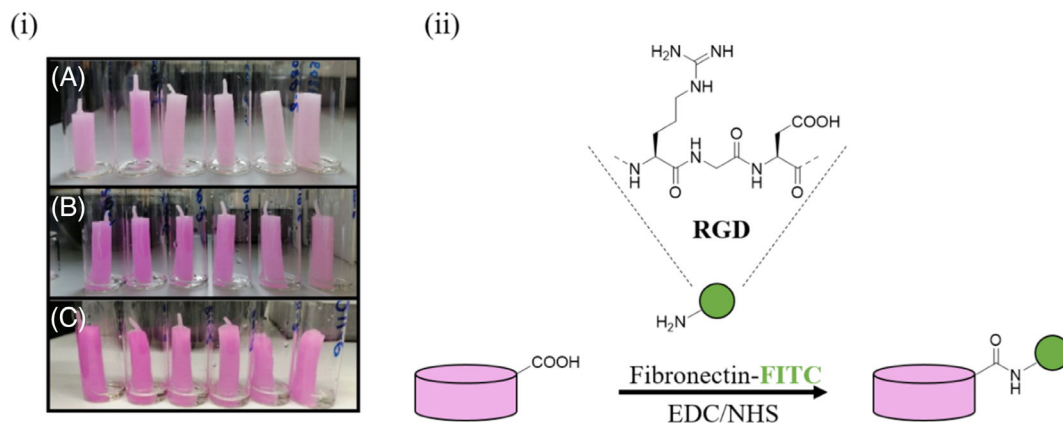


FIGURE 3 Panel (i): Series of duplicates of rhodamine B functionalized hydrophilic cryogels with different amounts of **MAG**. (A) Bisacrylamide cross-linked cryogels (**CGBis**). (B) **POx1** cross-linked cryogels (**CGPOx1**). (C) **POx2** cross-linked cryogels (**CGPOx2**). Panel (ii): Schematic representation of the fibronectin-FITC attachment to cryogels by EDC/NHS coupling.

investigated. Besides higher distances between the polymer chains resulting in enhanced flexibility of the gel network, it also allowed to introduce a higher degree of hydrophilicity due to the nature of poly(oxazoline)s. In general, six cryogels of each cross-linkers were prepared as duplicates for each of the three sugar quantities (26%/51%/76%) as well as their unfunctionalized cryogel analogues. For each cross-linker, cryogels were obtained as stable monoliths (Figure 3, panel (i)). An overview on the experimental conditions, amounts of reagents and gel fraction yields is given in Tables S1–S5.

Fibronectin-FITC was attached to an unfunctionalized cryogel sample (**CGPOx1-0**) as well as to a cryogel with sugar content (**CGPOx1-51**) by EDC/NHS coupling (Figure 3, panel (ii)) according to an adapted procedure from ThermoFisher.⁴⁵ The amount of attached protein was quantified by fluorescence measurements and was found to be 4.3 μg for **CGPOx1-0** and 6.5 μg for **CGPOx1-51** with a coupling efficiency of 26% and 40%, respectively (Table 3).

2.3 | Characterization of hydrophilic **MAG** cryogels

2.3.1 | Morphological investigations and pore size determinations

SEM images of all prepared cryogels revealed homogeneous pore structures and macroporous morphologies which was in accordance with the CLSM imaging results of cryogels measured in their native, hydrated state (Figures 4 and S3).

Notably, SEM and CLSM microscopy revealed various pore sizes based on qualitative observations. SEM images

of freeze-dried cryogel samples indicated the presence of smaller pores compared to the respective CLSM images of hydrated and swollen cryogels suggesting a shrinkage of pores during the freeze-drying process, as exemplary shown for **CGPOx1-26** which revealed a 2.8 times decrease of the median pore size in the dried state (Figure S4). For the determination of the pore sizes, we utilized an already established automated SEM image analysis platform which allows a fast and efficient evaluation of SEM images.⁴⁶ No clear correlation between cryogel pore sizes and the type of cross-linker or the sugar content was observed (Figure 5). The pore sizes varied between 18.5 and 23.0 μm , considering the median values. A full overview about the results of automated pore size measurements as well as the statistical analysis can be found in Tables S6 and S7 and Figure S5.

2.3.2 | Cryogel composition by ssNMR

ssNMR was applied to gain information about the cryogel composition and the successful incorporation of the sugar building block into the polymeric network. In comparison with the ^{13}C liquid NMR spectra of the corresponding monomers, the signals of the polymer side chains were assigned. For example, with increasing amount of **MAG** in the feed (from **CGBis-26** to **CGBis-76**), an increase in the signal intensities of the **MAG** peaks at 22 ppm (CH_3 group) and between 55 ppm and 100 ppm (CH groups) was observed in the ^{13}C ssNMR spectra for cryogels with bisacrylamide cross-linker (Figure 6).

In case of the unfunctionalized cryogel **CGBis-0**, no **MAG** related signals were visible. The decrease of the most intense signal at 42 ppm, belonging to the CH_3 groups of **DMAAm**, from **CGBis-26** toward **CGBis-76** is

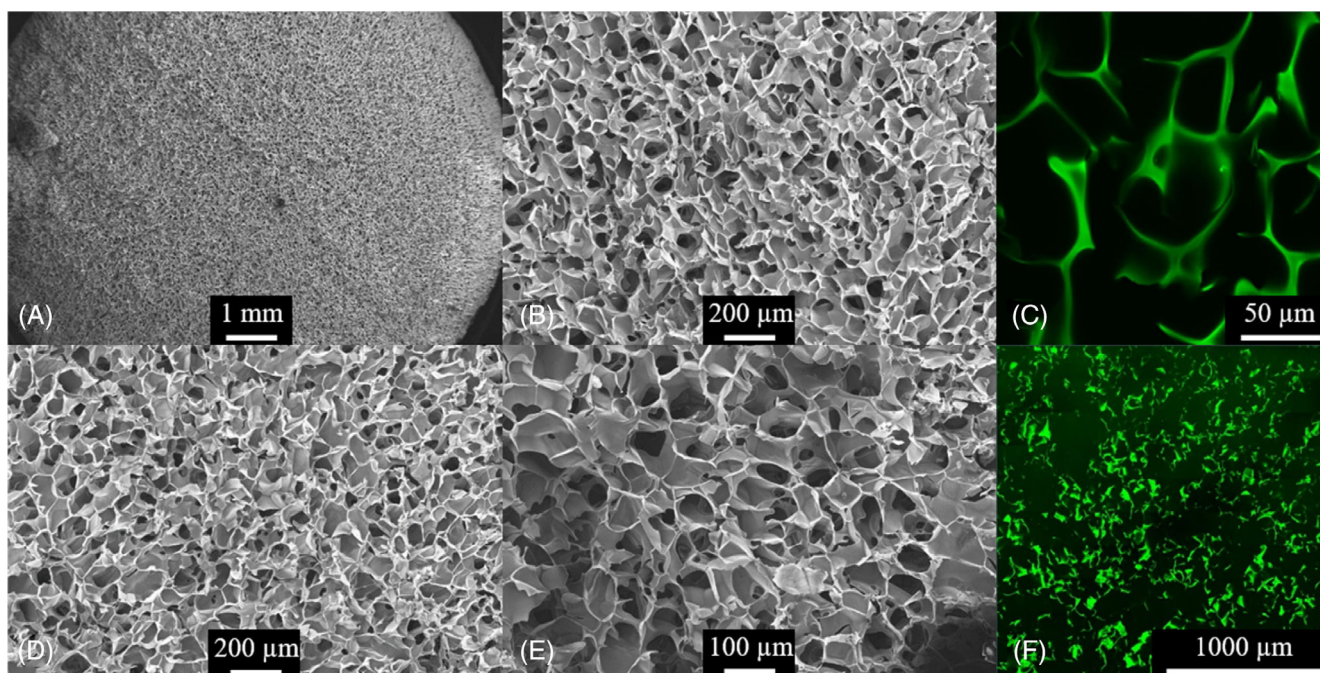


FIGURE 4 SEM micrographs with various magnifications of bisacrylamide cryogel **CGBis-26** (A: 12 \times ; B,D: 62 \times ; E: 128 \times) together with a detailed CLSM image (C) and a 10 \times 10 tile scan (F) obtained from CLSM.

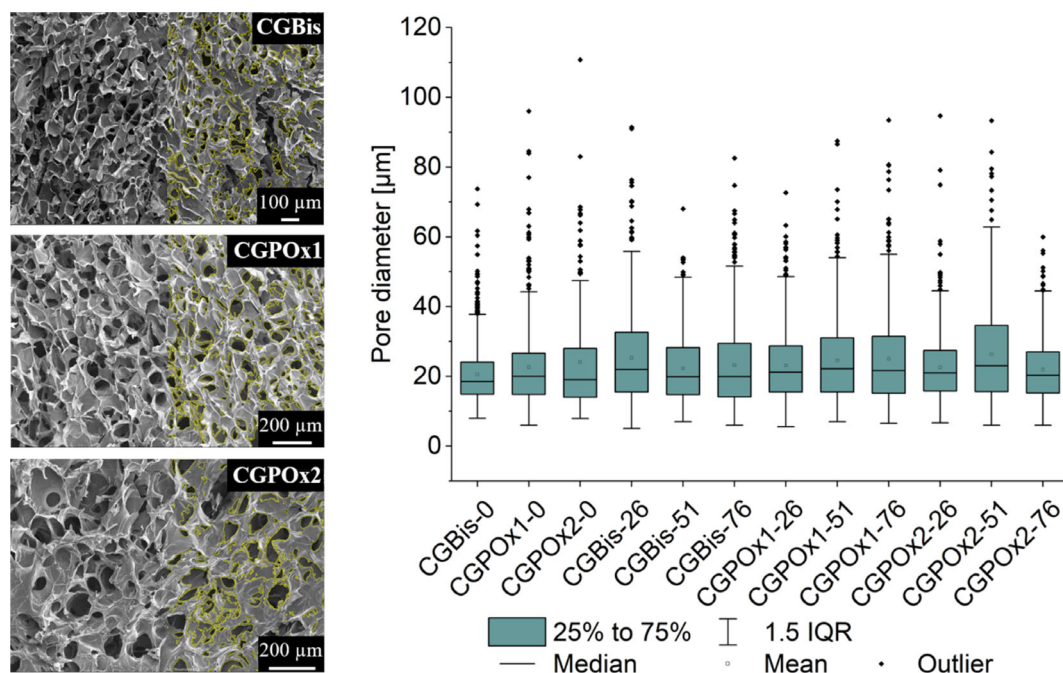


FIGURE 5 Left: Overlays of SEM images with algorithmic montages for the automated determination of the cryogel pores. Right: Box plots displaying the results of the pore size measurements based on the automated SEM image analysis for the entire cryogel series. The respective data can be found in Tables S6–S8. Boxes represent the position of 25% to 75% of the data with a 1.5 \times inter quartile range (IQR).

due to the reduced amount of **DMAAm** while increasing the amount of **MAG** in the feed. Furthermore, no signals between 120 and 140 ppm were observed in any cryogel spectra which would belong to the double-bond carbon

atoms of remaining unreacted monomers. Due to the absence of signals in this region and the presence of the side chain signals of the monomers in the cryogel spectra, the successful removal of potentially unreacted

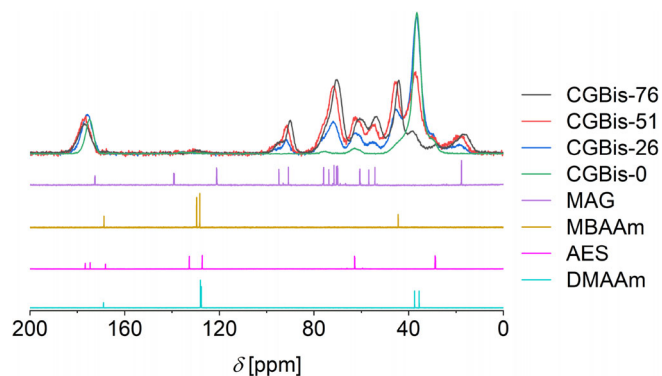


FIGURE 6 Stacked ^{13}C ssNMR spectra (400 MHz) of bisacrylamide based cryogels **CGBis-26** to **CGBis-76** (black, red, blue) and an unfunctionalized analogue **CGBis-0** (green) in comparison with the ^{13}C liquid NMR spectra (300 MHz, D_2O) of the corresponding monomeric building blocks: 2-(Methacrylamido) glucopyranose (purple, **MAG**), *N,N'*-methylene bisacrylamide (yellow, **MBAAm**), mono(2-acryloyloxyethyl) succinate (magenta, **AES**) and *N,N'*-dimethylacrylamide (cyan, **DMAAm**).

monomers and incorporation of all building blocks into the polymer gel network is demonstrated. The same trends were observed also in case of the **POx1** and **POx2** based cryogels (see Figures **S6** and **S7**). From that we conclude the successful preparation of cryogels with different amounts of **MAG** content as well as their unfunctionalized cryogel analogues per each of the three cross-linkers. In case of the poly(oxazoline) diacrylate cross-linked cryogels (**CGPOx1** and **CGPOx2** series), the very small signals between 120 ppm and 140 ppm can be assigned to the double bonds which belong to the DBB-derived initiator structure within the cross-linkers and might overlap with potentially remaining unreacted monomers. Due to the similar purification procedures after the reaction compared to the bisacrylamide cryogels, we assume that potentially unreacted monomers have been removed successfully also in case of the poly(oxazoline) diacrylate cryogels **CGPOx1** and **CGPOx2**.

2.3.3 | Analysis of functional groups using FTIR

FTIR was used to gain information of the composition and the presence of functional groups in the cryogels. Figure 7 summarizes the results exemplary for the bisacrylamide series **CGBis-26** to **CGBis-76** together with the unfunctionalized cryogel sample **CGBis-0**.

Most noticeably there is an increase in the intensities of the signals at 3300 cm^{-1} as well as 1000 cm^{-1} from **CGBis-0** towards **CG-Bis-76**. The strong and broad signal

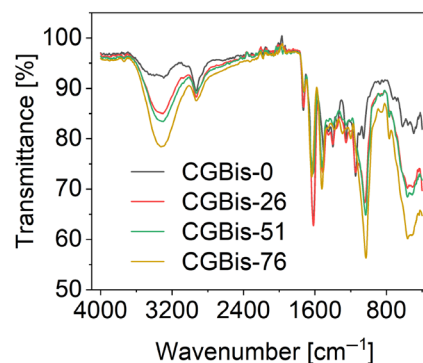


FIGURE 7 Stacked IR spectra of glucose functionalized bisacrylamide cryogels (**CGBis-26**, **CGBis-51**, **CGBis-76**) in comparison with an unfunctionalized analogue (**CGBis-0**).

at 3300 cm^{-1} is characteristic for alcohol moieties and can be explained by the O—H stretching vibration, whereas the signal at 1000 cm^{-1} can be interpreted as C—O stretching vibration of primary or secondary alcohol functions. The increase of the signal intensities strongly indicate the successful incorporation of increasing amounts of **MAG** into the cryogel network. The same trend can be observed from the poly(oxazoline) cryogel series **CGPOx1-26** to **CGPOx2-76** (see Figures **S8** and **S9**). Nevertheless, the increase of the OH vibration band is less pronounced compared to the bisacrylamide series. Since the molar monomeric concentration was kept constant throughout the entire series of cryogels (**CGBis** to **CGPOx2**), the amount of **MAG** in the feed dropped with increasing molar mass of the cross-linker. Since less amount of **MAG** was used for the **POx1** and **POx2** cryogels, the signals are less intense for these systems.

2.3.4 | Determination of the thermal properties by TGA

TGA was performed in order to investigate the thermal properties of the cryogels (Figure 8).

For the sugar containing cryogels **CGBis-26** to **CGBis-76** the first derivative curves show two major transitions at approximately $220\text{ }^\circ\text{C}$ as well as at approximately $400\text{ }^\circ\text{C}$ before reaching almost complete decomposition at approximately $450\text{ }^\circ\text{C}$. In each of the three cryogel series (**CGBis**, **CGPOx1**, and **CGPOx2**), the degradation curve is getting steeper between $200\text{ }^\circ\text{C}$ and $400\text{ }^\circ\text{C}$ with increasing theoretical amount of **MAG** resulting in an increase of the area of the first transition peak at $220\text{ }^\circ\text{C}$ in the first derivative curves. In comparison with the unfunctionalized cryogel **CGBis-0** it could be clarified for the bisacrylamide cryogels that the first transition peak is caused by the **MAG** portion and its

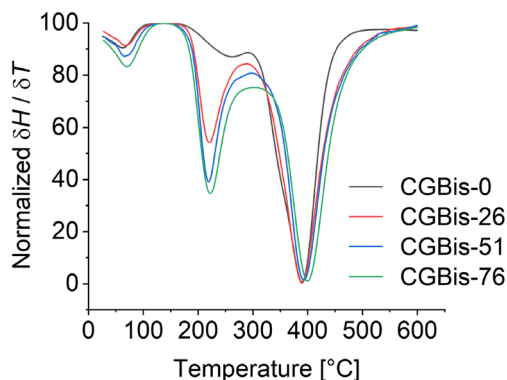


FIGURE 8 Overview about the first derivative TGA degradation curves of glucose functionalized bisacrylamide cryogels (**CGBis-26** to **CGBis-76**) in comparison with an unfunctionalized cryogel **CGBis-0**.

degradation as the peak intensity is increasing with increasing amount of **MAG** in the feed. In case of **CGBis-0**, there is only one major transition at approximately 400 °C visible. Thus, incorporation of **MAG** seems to decrease the thermal stability of the gels. Nevertheless, due to their thermal stability up to 150 °C, all cryogels are applicable for autoclaving prior to culture experiments. For the **POx1** and **POx2** cross-linked gels, the same trends could be observed (see Figures [S10](#) and [S11](#)). Due to the reduced amount of **MAG** with increasing molar mass of the cross-linker in the feed, the influence of **MAG** on the thermal properties is decreasing towards the **POx2** cryogel series which is indicated by the decreasing area of the first peak.

2.3.5 | Impact of the autoclaving procedure on the gel properties

ssNMR and TGA were applied to investigate the gels' integrities after autoclaving treatment exemplary to the gels with the highest theoretical amount of **MAG** for each of the three cross-linkers. By the use of ^{13}C ssNMR, we could not observe major alterations in the spectra, as they were almost identical, independently of the cross-linkers (Figure [9](#), panel (i), Figures [S12](#) and [S13](#)).

From the TGA curves, a slight change in the curve progressions was observed, which decreased with increasing molar mass of the respective cross-linker from **CGBis-76** to **CGPOx2-76** (Figure [9](#), panel (ii), Figures [S14](#) and [S15](#)). From that we conclude that there are no changes in the chemical structure of the cryogels caused by autoclaving. In addition, CLSM and SEM images were taken of selected cryogel samples from each cross-linker series before and after autoclaving to observe a potential influence on the cryogel morphologies

(Figure [9](#), panels (iii) and (iv), Figure [S16](#)). It could be demonstrated from CLSM and SEM imaging that the pore structure after autoclaving did not exhibit any severe damages like ruptures, remained intact and were comparable with images before the autoclaving which furthermore underlines the capability of the cryogels to resist autoclaving.

2.4 | Cell culture experiments

FM and CLSM were applied to investigate the cell morphologies and the cellular penetration depths into the cryogel materials following incubation. For this purpose, L929 cells were cultivated on top of the gels. The gels were tightly fitting to the sidewalls of the sterile syringes preventing a cell sedimentation aside the cryogels (Figure [10](#), panel (i)).

No morphological abnormalities of the cell shapes as e.g. vesicle formation, membrane blebbing or disruption as signs for apoptotic or necrotic effects were observed by CLSM, as exemplary shown in Figure [10](#), panel (ii) for **CGPOx1-26** and **CGPOx2-0**. An overview of the CLSM images of the remaining samples from the whole series can be found Figures [S17–S19](#). The nuclei and the cytoplasmic areas were well recognizable and clearly demarcated suggesting healthy cells within the surrounding cryogel environment. Cells were forming three-dimensional aggregates within the cryogel pores as visualized by the respective CLSM images.

The determination of the cell penetration depth based on merged tile images from fluorescence microscopy revealed the presence of L929 cells in deeper cryogel sections with increasing **MAG** content of the materials, which is shown exemplary in Figure [11](#), panel (i) for representative cryogel samples selected from the entire series (**CGPOx2-0** and **CGPOx2-76**). This trend was consistent among the entire cryogel series. The corresponding cellular penetration depths can be found in Table [2](#).

FM imaging of selected fibronectin coupled cryogel samples revealed a sedimentation of the L929 cells on the cryogel top surface without a further settlement into deeper cryogel zones during the incubation (Figure [11](#), panel (ii)). This might indicate the influence of the protein on promoting the cellular adhesion compared to the glucose containing surfaces which rather support deeper cellular settlements based on sedimentation or active migration in the cryogels. In literature, there are not so many examples in which cellular settlements has been evaluated depending on cryogel surface functionalization. In a study from Bahlmann *et al.*, the functionalization of bio-polymer based gelatin-hyaluronic acid cryogels with an

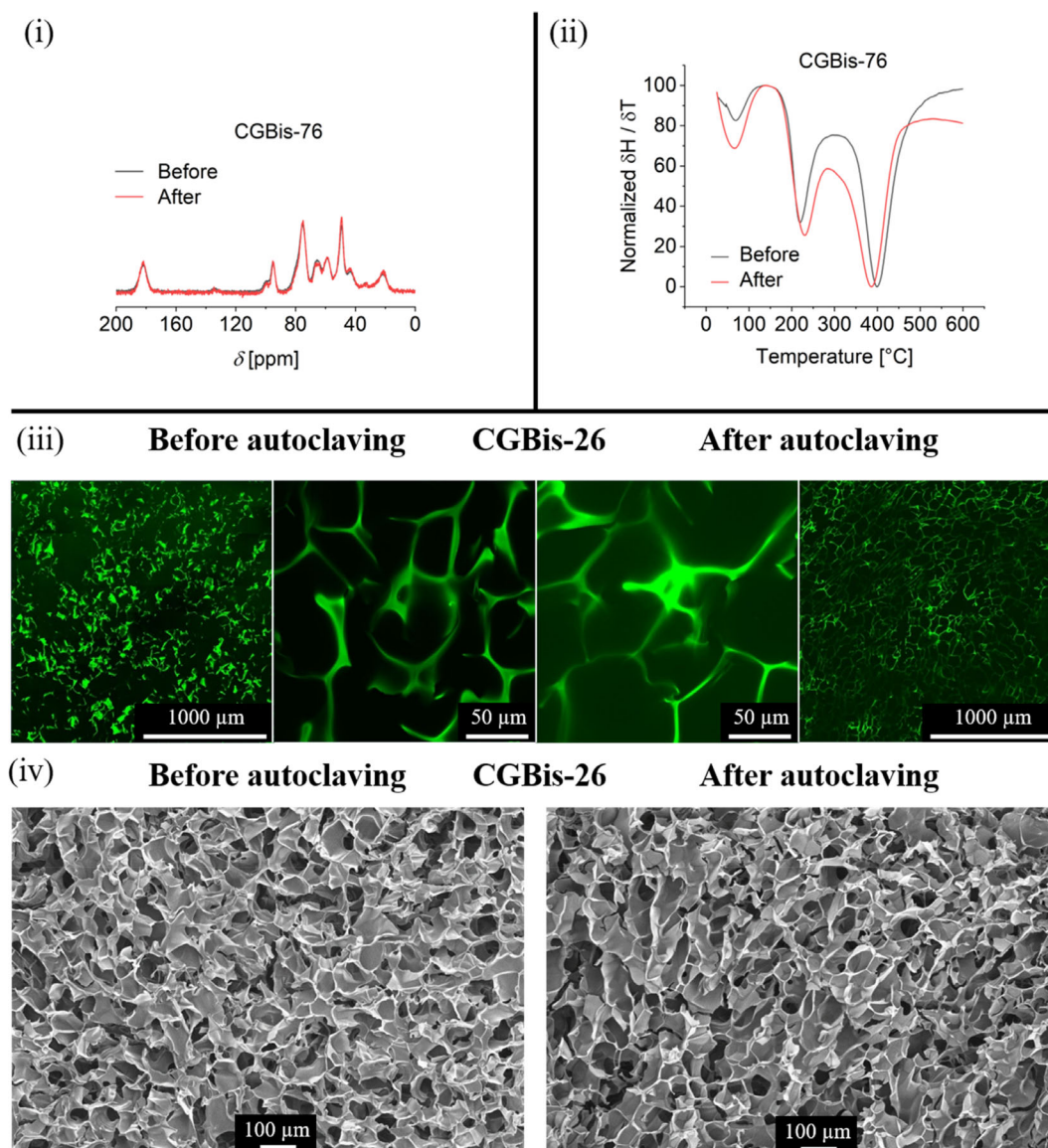


FIGURE 9 Panel (i): ^{13}C ssNMR spectra (400 MHz) of a bisacrylamide cryogel containing a theoretical amount 76% of **MAG** (**CGBis-76**), before and after autoclaving procedure. Panel (ii): First derivative TGA curves of a bisacrylamide cryogel containing a theoretical amount 76% of **MAG** (**CGBis-76**), before and after autoclaving procedure. Panel (iii): Overview about the pore structures of bisacrylamide cryogel with 26% **MAG** content (**CGBis-26**) before and after autoclaving. CLSM images are displayed as 10×10 tile scans (left and right column) as well as detailed images (two middle columns). Panel (iv): SEM micrographs of **CGBis-26** before and after autoclaving.

RGD peptide sequence (PHSRN-RGDSP) significantly improved the settlement of human macrophages into the cryogels compared to unfunctionalized analogues.⁴⁷ However, our studies with fibroblasts based on synthetic polymer based p(MAG) cryogels revealed a deeper settlement depending on the **MAG** content and a retention of cells with additional fibronectin coating. We believe that the observed difference in the cellular settlement behavior compared to the study by Bahlmann *et al.* is mostly due to different cell culture conditions such as the cell type as well as the different nature of the used cryogel materials.

2.5 | Metabolic activity

Examples in literature evaluated the viability of cells after incubation on cryogels with quantitative approaches measuring the metabolic activity of cells based on MTT assay,^{48–53} XTT assay,⁵⁴ neutral red uptake assays⁵⁵ or rather qualitative microscopic setups with live/dead staining.^{49,50,56} All examples mentioned were performed in two-dimensional well plates, whereas we decided to perform cell viability studies in a three-dimensional syringe based setup according to the cell culture experiments for microscopic evaluations. Herein, we used an

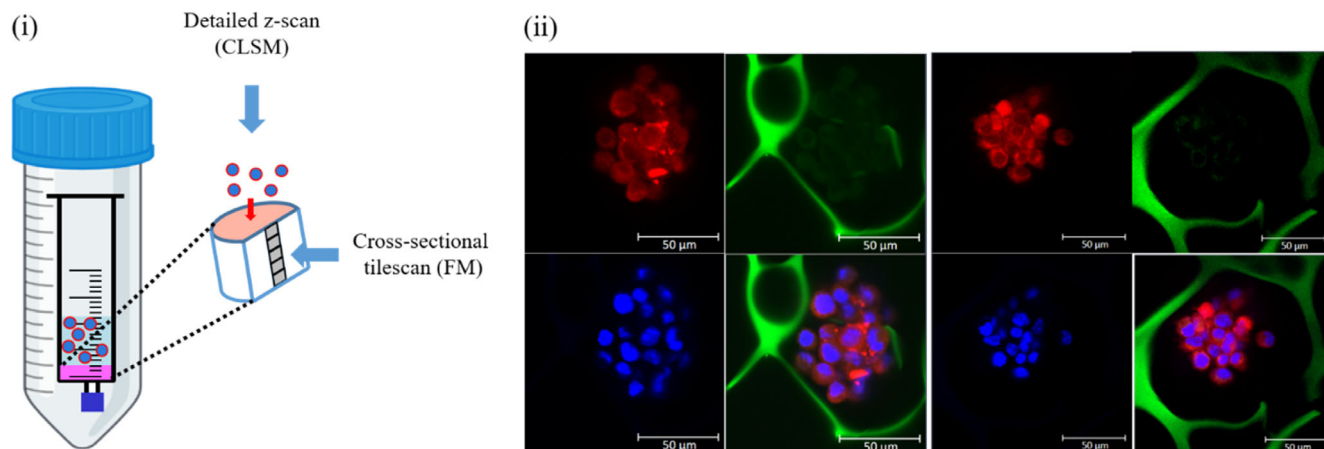


FIGURE 10 Panel (i): Schematic representation of the cultivation of L929 cells on hydrophilic cryogels using a syringe setup. Cells were pre-stained before cultivation with Hoechst 33258 and CellTracker™ Deep Red to label the nuclei (blue) and the cytoplasm (red), respectively. A detailed z-scan from the top and a cross-sectional tile scan were recorded using CLSM or FM, respectively. Panel (ii): Exemplary CLSM images of L929 cells cultured on **POx1** (left) and **POx2** (right) based cryogels (**CGPOx1-26** and **CGPOx2-0**) with different portions of **MAG** (26% and 0%, respectively). Cells were pre-labeled before the cultivation with CellTracker™ Deep Red (cytoplasm, A and E, red) and Hoechst 33258 (nuclei, C and G, blue). The cryogel network appears green due to rhodamine B incorporation (B and F). Overlay images (D and H) depict L929 cells in a cryogel pore. An overview about the CLSM images of the other remaining cryogels can be found Figures S16–S18.

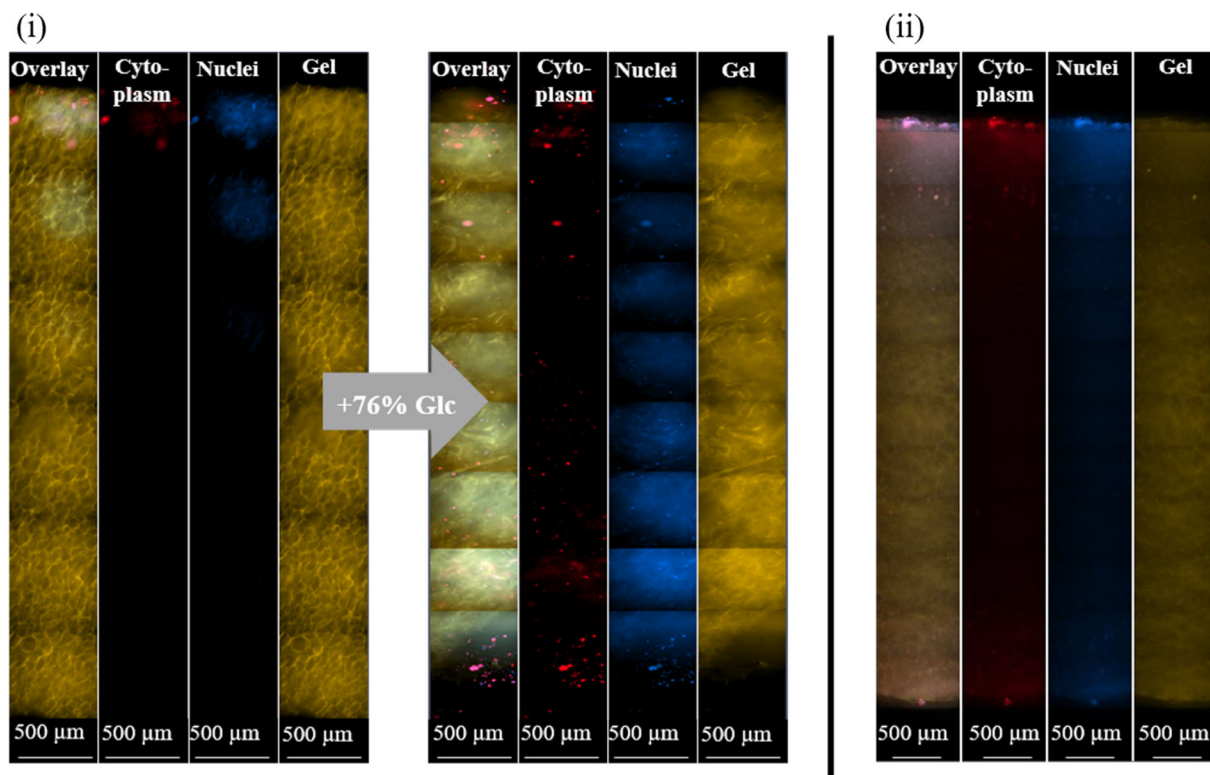


FIGURE 11 Panel (i): Cross-sectional cryogel micrographs of two selected **POx2** based cryogels either without sugar (**CGPOx2-0**) or with 76% sugar incorporation (**CGPOx2-76**) visualizing the cell-penetration depth into the cryogel materials after incubation. Cellular cytoplasm was stained with CellTracker™ Deep Red and the nuclei were labeled with Hoechst33258. Panel (ii): Cross-sectional cryogel micrographs of fibronectin-FITC functionalized cryogel **CGPOx1-51** visualizing the overall structure, the cellular cytoplasm stained with CellTracker™ Deep Red, the Hoechst labeled nuclei and the gel scaffold labeled with rhodamine B.

TABLE 2 Penetration depths of L929 cells into hydrophilic cryogels depending on the different amounts of sugar incorporation (from 0% up to 76%) and cross-linker type (**Bis**, **POx1**, or **POx2**) were manually measured from the top of the cryogel to the location with the highest abundance of cells.

	0% (μm)	26% (μm)	51% (μm)	76% (μm)
CGBis	550	1400	1800	800/1800
CGPOx1	400	3500	1400	1800/2250
CGPOx2	450	640/1500	3500/6000	2600/4000

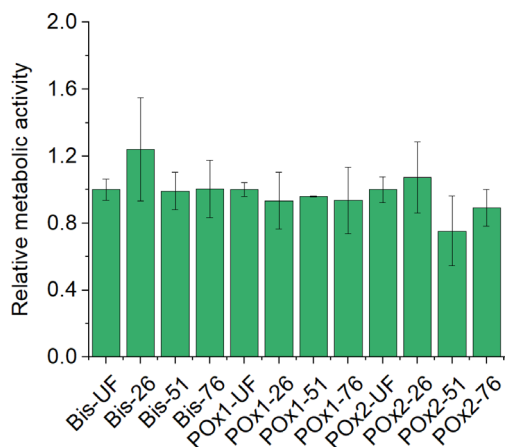


FIGURE 12 Metabolic activity of cells cultured with cryogels using different cross-linkers.

adapted alamar blue assay which quantifies the metabolic activity of the cultured cells. The aim was to investigate the relative metabolic activities of the cells depending on the different cryogel scaffolds which are summarized in Figure 12.

The relative metabolic activities of L929 cells cultured on the differently modified cryogels were found to be all in a similar range between 0.75 and 1.24. No significant differences between the mean values of the relative metabolic activities among the cryogel series were observed. There was no clear trend or dependency regarding the amount of sugar or the type of cross-linking. In combination with cell morphological images from CLSM which revealed the presence of healthy cells after incubation and no signs of cellular damage or apoptosis (Figure 10, panel (ii)) we assume the absence of cytotoxic effects caused by the tested cryogels.

3 | CONCLUSION

Glucosamine functionalized cryogels were successfully prepared and characterized regarding their composition, thermal properties, and morphology. Solid-state NMR

and IR visualized the incorporation of various amounts of **MAG** in each of the three cryogel series. SEM imaging demonstrated homogenous morphologies and regular pore structures with pore sizes in the range of 18.5–23.0 μm as determined by automated image analysis. TGA measurements revealed thermal stabilities of all synthesized gels up to 180 $^{\circ}\text{C}$ indicating their potential of withstanding sterilization via autoclaving treatment prior to the cell culture experiments. TGA and ssNMR measurements of samples before and after autoclaving further underlined that no significant change in the chemical composition of the gels is occurring. In addition, CLSM imaging did not show any observable structural changes in the cryogel morphologies (with pore sizes in the swollen state of 50–100 μm). L929 fibroblast cells were cultivated within the prepared cryogels and the cellular morphologies as well as the cellular settlements in the cryogel matrices were observed by CLSM and FM. CLSM revealed healthy cells within the cryogel scaffolds after incubation. With increasing **MAG** content of the cryogels, cells settled deeper into the materials. After attachment of the cell-adhesion promoting protein fibronectin, the L929 cells were retained much stronger and stayed at the top layers of the gels. According to the intact cellular morphologies and the different cellular settlements of the cells depending on the surrounding microenvironment, we are convinced that our basic but encouraging cell culture studies are an excellent starting point for further experiments in order to use the prepared cryogels as 3D culture materials, for example, to study the cultivation of cells, tumor invasion or cancer cells migration as well as immune cell-microbe interactions.

4 | EXPERIMENTAL SECTION/ METHODS

4.1 | Materials

Prior to the polymerizations, *N,N*-dimethylacrylamide (DMAAm, 99%, Sigma Aldrich) and mono (2-acryloyloxethyl) succinate (AES, 90%, TCI) were passed through a small column filled with inhibitor removal beads (replacement packing for removing hydroquinone and monomethyl ether hydroquinone, Sigma Aldrich). *N,N,N',N'*-Tetramethylethylenediamine (TMEDA, 99%), *N*-hydroxysuccinimide (NHS, 98.0%), sodium phosphate tri-basic dodecahydrate (ACS reagent, > 98.0%) and fibronectin-FITC (1 mL of 1 mg mL⁻¹ solution) were purchased from Sigma Aldrich. Potassium peroxodisulfate (K₂S₂O₈, ≥ 98%) was purchased from Fluka Analytical. *N,N'*-Methylenebisacrylamide (MBAAm, > 99%) was purchased from Alfa Aesar. Glucosamine hydrochloride

(98.0%) and 1-(3-dimethylaminopropyl)-3-ethylcarbodiimide (EDC, >98.0%) were purchased from TCI. Acryloxethyl thiocarbonyl rhodamine B (ATRB) was purchased from Polysciences. Potassium carbonate (99%) was purchased from Grüssing GmbH. Sodium chloride was received from Fisher Scientific ($\geq 99.5\%$). 2-(*N*-Morpholino)-ethanesulfonic acid (MES, $\geq 99\%$) was purchased from Carl Roth. Anhydrous methanol was obtained using a solvent purification system (MB-SPS-800 by MBraun). MES activation buffer was freshly prepared from MES (0.1 M), NaCl (0.5 M) and millipore water and was adjusted to pH 6.0. PBS buffer was directly prepared from $\text{Na}_3\text{PO}_4 \times 12 \text{H}_2\text{O}$ (0.1 M) and NaCl (0.15 M) and was adjusted to pH 7.2. All other chemicals were purchased from standard suppliers and were used without any further purification unless otherwise stated. Poly(2-ethyl-2-oxazoline) diacrylate macromolecular cross-linkers **POx1** (DP10) and **POx2** (DP20) were previously synthesized by cationic ring-opening polymerizations of 2-ethyl-2-oxazoline using *trans*-1,4-dibromobut-2-ene as initiator which was described earlier.⁴³ In all cryogel preparations, ultrapure water (Merck Millipore water purification system) was used unless otherwise stated. For a precise and adjustable control of the reaction temperature for the cryopolymerization reactions, a cryostat was used (Julabo FP40-MC, Julabo GmbH, Seelbach, Germany). Cell culture reagents DMEM, fetal bovine sera, penicillin, streptomycin, trypsin were purchased from Biochrom, Cell dyes Hoechst 33258 and CellTracker™ Deep Red were purchased from ThermoFisher Scientific.

4.2 | Instrumentation

Proton NMR spectra (^1H NMR) and carbon NMR spectra (^{13}C NMR) were recorded using a 300 MHz Advance I spectrometer equipped with a dual ^1H and ^{13}C probe head and a 120 \times BACS automatic sample changer (Bruker, Germany). The residual ^1H peak of the deuterated solvent was used for chemical shift referencing, chemical shifts are given in parts per million (ppm). ^{13}C solid-state NMR spectra were recorded using a 400 MHz Bruker Advance III HD spectrometer with a 4 mm MAS probe head. Cryogel micrographs for morphological investigations and pore size measurements were obtained using a Sigma VP Field Emission Scanning Electron Microscope (Carl Zeiss, Jena, Germany) with an SE-2 detector and an accelerating voltage of 10 kV was used. For this purpose, freeze-dried cryogel slices were obtained using the freeze dryer Alpha 2–4 LD plus (Martin Christ) before they were coated with a 9 nm platinum layer using a CCU-010 HV sputter coater

(Safematic, Zizers, Switzerland) and fixed onto the plate holder pins with glue pads. An automated image analysis algorithmic approach (JIPipe) was applied to obtain cryogel pore sizes from selected SEM images. A full view picture of the entire sample was taken before taking selected views with higher magnifications. Electrospray-ionization mass spectrometry (ESI-MS) was performed with a microTOF Q-II from Bruker Daltonics which was equipped with an automatic syringe pump from KD Scientific. The ESI-Q-ToF mass spectrometer was operating at 4.5 kV in the positive ion mode and at a desolvation temperature of 180 °C. Nitrogen was used as the nebulizer and drying gas. Sample injection was performed using a constant flow rate of 3 $\mu\text{L min}^{-1}$. The instrument was calibrated in the m/z range 50 to 3000 using a calibration standard (ESI-L Low Concentration Tuning Mix), which was supplied from Agilent Technologies. The data were processed via Bruker Data Analysis software version 5.3. Trapped ion mobility mass spectrometry (TIMS) was performed using a trapped ion mobility quadrupole time-of-flight mass spectrometer (timsTOF, Bruker Daltonics). The instrument was operating at 3.6 kV in the positive mode and at a desolvation temperature of 200 °C using nitrogen as the nebulizer and drying gas. The samples were injected using a constant flow rate of 3 $\mu\text{L min}^{-1}$ of the sample solution. Spectra were recorded from 100 to 3000 m/z and ion mobility scanned from 0.6 to 2.0 Vs cm^{-2} . The instrument was calibrated in the m/z range 80–2000 (Tune_pos-Standard_avg) using a calibration standard (ESI-L Low Concentration Tuning Mix, Agilent Technologies). All data were processed via Bruker Data Analysis software version 5.1. Thermogravimetric analysis (TGA) was carried out under nitrogen atmosphere using a Netzsch TG209 F1 Libra (Selb, Germany). For the measurements, a standard method was used (25–600 °C with a heat rate of 20 K min^{-1} , 29 min). After the measurements, smoothing was applied as post processing step if necessary. Fourier-transform infrared (FT-IR) spectra were recorded from 400 to 4000 cm^{-1} using an IR-Affinity-1 CE system (Shimadzu, Kyoto, Japan) which was equipped with a quest ATR diamond extended range X-single reflection-ATR accessory with a diamond crystal. The spectra were smoothed after the measurements if necessary. Fluorescence intensity measurements were carried out using an Infinite M200 PRO microplate reader (Tecan) at 490 nm (λ_{Ex}) and 520 nm (λ_{Em}). Cryogels for cell cultivation experiments and for thermal stability studies were autoclaved in water containing glass-vials with a Systec VX-180 autoclave for 20 min at 120 °C and 2.1 atm pressure.

Microscopic evaluation of cryogels cultured with L929 cells was performed using the confocal laser scanning microscope LSM880 Elyra PS.1 system

(Zeiss, Oberkochen, Germany) with a C-Apochromat 40×/1.2 W Korr FCS M27 objective and the epifluorescence box microscope Celldiscoverer CD7 (Zeiss, Oberkochen, Germany) with a Plan-Apochromat 20×/0.7 with 0.5× Optovar objective. Images were acquired and analyzed using the ZEN software. Determination of cell penetration depth was performed by the manual evaluation of fluorescence microscopy images using ImageJ software.

4.3 | Synthesis of the POx-based cross-linkers POx1 and POx2.

The synthesis and characterization of poly(2-ethyl-2-oxazoline) diacrylate cross-linkers with a DP of 10 and 20 was already described in a previous work.⁴³

4.4 | Synthesis of 2-(methacrylamido) glucopyranose (MAG).

2-(Methacrylamido) glucopyranose was synthesized according to a literature procedure.⁴⁴ To a suspension of glucosamine hydrochloride (10.02 g, 46.47 mmol) and potassium carbonate (10.0 g, 72.35 mmol) in methanol (100 mL), methacryloyl chloride (5 mL, 51.18 mmol) was added with a syringe pump (World Precision Instruments, Sarasota, FL, 0.5 mL min⁻¹) at -10 °C. The reaction mixture was allowed to reach room temperature and stirred overnight before removing residual solids by filtration. Silica gel was added to the filtrate and the solvent was evaporated under reduced pressure. The pure product was obtained by column chromatography (SiO₂, CH₂Cl₂:CH₃OH = 4:1) as a mixture of α and β anomers as a white powder (3.94 g, 34% yield).

¹H NMR [ppm] (D₂O, 300 MHz): δ = 1.92 (CH₃, 6H), 3.36–4.00 (m, 12H), 4.75 (β -CH), 5.21 (α -CH, d, 3.42 Hz, 1H), 5.46 (CH₂, s, 2H), 5.69 (CH₂, s, 2 H).

¹³C NMR [ppm] (D₂O, 300 MHz): δ = 17.7, 17.8, 54.3, 56.9, 60.6, 60.8, 69.9, 70.1, 70.5, 71.6, 73.7, 75.9, 90.8, 94.9, 121.1, 121.2, 139.1, 172.5, 172.6.

HR-MS (ESI): calculated for C₁₀H₁₇NO₆Na: 270.0948, found 270.0947 ([M + Na]⁺).

TIMS: 270.0945 (peak 1, ion mobility of 1.01 Vs cm⁻²), 270.0947 (peak 2, ion mobility of 0.76 Vs cm⁻²).

4.5 | General preparation of hydrophilic cryogels (CGBis to CGPOx2)

A solution of (macro-) monomers together with K₂S₂O₈ in Millipore water was prepared and filled into a 5 mL

polypropylene syringe which was bottom-capped with a syringe stopper. The solution was purged with argon for 30 min at 0 °C before an aqueous TMEDA solution was added. Subsequently, the syringe was closed with the plunger followed by vortexing for 10 seconds and was placed in a cryostat bath (-13 °C). Cryopolymerization was carried out for 20.5 h. Afterwards, the syringe was removed from the bath and thawed at room temperature for 1 h. The resulting cryogel was removed and immersed in water/methanol to remove unreacted monomers. The solvent was replaced at least once every day for three to 5 days. The monoliths were cut into slices using a steel blade followed by freeze-drying for at least 2 days. One slice was used for SEM imaging analysis whereas three to four slices were ground to a fine powder for ssNMR, IR, and TGA analysis. A summary of all the prepared cryogels including conditions and the exact amounts of the chemicals used is given in Tables S1–S4.

4.6 | General procedure of fibronectin attachment to the cryogels

A freeze-dried cryogel slice was placed in a 5 mL polypropylene syringe followed by the addition of MES activation buffer (0.1 M MES, 0.5 M NaCl, adjusted to pH 6; 3 mL). The soaked gel slice was washed several times with fresh buffer. Subsequently, a solution of EDC and NHS in activation buffer (2 mL) was added and the passed eluate was added on top of the slice again to pass through for at least three consecutive runs. Subsequently, the solution was removed before adding 2 mL of a diluted fibronectin-FITC solution (1 mg mL⁻¹ diluted to 0.033 mg mL⁻¹ with PBS buffer [0.1 M Na₃PO₄, 0.15 M NaCl, pH 7.2]). The protein solution was allowed to pass through the gel slice for at least five times before bottom-capping the syringe with a syringe stopper. The protein solution was added and allowed to react for 16 h at 4 °C protected from light. Afterwards the solution was passed through for three more times before washing the gel slice with PBS buffer (4 × 2 mL). Each wash fraction was collected separately for fluorescence analysis. The amount of bound protein was determined using fluorescence spectroscopy by measuring the initial protein concentration and the concentration in solution after the coupling including the residual protein amounts after each washing step. An overview about the exact experimental details for all the coupling experiments is given in Table 3. For fluorescence intensity measurements, a calibration curve was recorded consisting of 10 different protein concentrations in the range of 0.033 mg mL⁻¹ to 0.260 μ g mL⁻¹.

TABLE 3 Overview about conditions used for the coupling of fibronectin-FITC to hydrophilic cryogels.

	$m_{\text{CG slice}}$ (mg)	$n_{\text{COOH,theo}}$ (mmol)	m_{NHS} (mg)	V_{EDC} (μL)	V_{protein} (mL)	$m_{\text{protein,bound}}$ (μg)	$m_{\text{protein,feed}}$ (μg)	Coupling efficiency (%)
499-2 CGPOx1-0-1	28	0.014	43	25	2	33.7	67.2	50
499-3 CGPOx2-0-1	28	0.009	30	18	2	23.0	70.6	33
499-5 CGPOx1-0-2	22	0.015	48	27	2	31.9	67.2	47
499-6 CGPOx2-0-2	20	0.010	31	18	2	32.7	70.6	46
499B2-1 CGPOx1-0-3	28	0.010	22	12	1	5.6	16.3	34
499B2-2 CGPOx1-0-4	30	0.010	23	13	1	4.3	16.3	26
510-5A CGPOx1-76-1	25	0.008	23	14	2	33.1	67.2	49
510-5B CGPOx1-76-2	22	0.006	20	11	2	35.8	67.2	53
511-5A CGPOx2-76-1	24	0.007	18	10	2	34.0	70.6	48
511-5B CGPOx2-76-2	31	0.005	19 g	11	2	38.4	70.6	54
510-3 CGPOx1-51-1	28	0.008	23	14	1	8.5	16.3	52
510-4 CGPOx1-51-2	27	0.008	23	15	1	6.5	16.3	40

Note: $m_{\text{CG slice}}$ = Mass of the respective cryogel slice. $n_{\text{COOH,theo}}$ = Theoretical amount of substance of carboxylic acid groups per cryogel slice. Coupling efficiency is expressed as the ratio of bound protein divided by the initially used amount before the coupling.

4.7 | Image analysis and pore size measurements

Pore size measurements were carried out based on the evaluation of SEM images. By the use of a deep learning-based algorithm established in JIPipe,^{57–59} the cryogel pore sizes were automatically measured using four images per sample. Only the median values were considered as reliable measures to compare the pore size variation among the cryogel series. The establishment and creation of the algorithmic approach was described in an earlier work.⁴⁶ In brief, electron microscopy images were analyzed in TIFF 8-bit format, using a workflow written in JIPipe.⁵⁹ The analysis produced intensity-based and morphometric measures of the pores; the latter was also utilized to compare the automated framework of analysis with the manual measurements of the pores. The analysis was carried out by exploiting deep-learning (DL) methods. We applied the JIPipe implementation of the Cellpose framework after appropriate transfer learning.⁶⁰

4.8 | Cell culture experiments

Prior to the cultivation experiments, L929 fibroblast cells were routinely cultured as follows: Dulbecco's modified eagle's medium (DMEM) supplemented with 10% fetal calf serum (FCS), 1 g L⁻¹ glucose, 100 U mL⁻¹ penicillin and 100 $\mu\text{g mL}^{-1}$ streptomycin (D10F+, all components from Biochrom, Berlin, Germany) at 37 °C in a humidified atmosphere with 5% (v/v) CO₂. After cell detachment using trypsin treatment, the cells were suspended in serum free DMEM (4 × 10⁶ cells mL⁻¹) containing Hoechst 33258 (1 $\mu\text{g mL}^{-1}$) and CellTracker™ Deep Red (10 μM) and were incubated at 37 °C for 30 min to label the nuclei and cytoplasm, respectively. After centrifugation cells were resuspended in D10F+ to yield a cell concentration of 4 × 10⁵ cells mL⁻¹. The cryogel slices were equilibrated in D10F+ for 1 h and subsequently transferred into 5 mL polypropylene syringes carrying a bottom cap. Four milliliters of the cell suspension were applied onto the cryogels (1.6 × 10⁶ cells per cryogel). After adding the cell suspension, syringes were transferred to a

50 mL falcon tube which was loosely capped to ensure gas permeation. The following incubation was carried out at 37 °C for 48 h in a humidified atmosphere with 5% (v/v) CO₂. Next, the suspension was carefully aspirated and the cells were fixed on the gels for 2 h using 2 mL 4% paraformaldehyde solution. The fixation solution was removed and the cryogels were taken out of the syringe before vertically cutting in halves with a scalpel. The gel slices were transferred into 24-well microscope plates (Ibidi GmbH, Gräfelfing, Germany) either topside down or with the cross-section downwards the dish bottom followed by the addition of PBS buffer to avoid drying of the slices. A cross-sectional tile scan and a z-scan was taken using the Celldiscoverer 7 fluorescence microscope. By the use of confocal laser scanning microscopy, a detailed z-scan from the topside of the cryogel was acquired.

4.9 | Cell viability assay

For assessing the metabolic activity of L929 fibroblast cells following incubation with cryogels, samples were prepared as described for microscopic analysis except the cellular staining. After 24 h incubation, AlamarBlue stock solution (400 µL of 10 v%) was directly added and the syringe was shortly inverted for homogenization. A further incubation was carried out at 37 °C for 4 h. The supernatant was removed and transferred into a 12 mL Falcon tube followed by centrifugation. Aliquots of the supernatant (6 × 100 µL) were transferred to a 96 well plate and subjected for fluorescence intensity measurements. This experiment was performed in triplicate.

4.10 | Statistical analysis

Cryogel pore sizes were compared using the Kruskal–Wallis analysis of variances (ANOVA) as well as Mood's median test. Statistical significance was set at $p < 0.05$. Differences between test groups were assessed in both methods using Dunns test. Absolute metabolic activities were obtained from fluorescence intensity measurements. All of the three data sets (CGBis, CGPOx1, and CGPOx2) were then divided by the values of the corresponding unfunctionalized cryogels (CGBis-0, CGPOx1-0, or CGPOx2-0) to obtain the relative metabolic activities. Comparisons between the relative metabolic activities of the different cryogel samples were performed using one-way ANOVA. Differences between test groups were assessed using Tukey and Levene tests. Statistical significance was set at $p < 0.05$.

ACKNOWLEDGMENTS

The authors thankfully acknowledge Leon Lange for ssNMR measurements and Nicole Fritz for ESI-MS and TIMS-TOF measurements. This work was funded by the Deutsche Forschungsgemeinschaft (DFG, German Research Foundation, project number: 390713860, 316213987, SCHU 1229/25-1, LI 916/19-1 and GO 1100/4-1). The SEM facilities of the Jena Center for Soft Matter (JCSM) were established with a grant from the DFG. Open Access funding enabled and organized by Projekt DEAL.

CONFLICT OF INTEREST STATEMENT

The authors declare no conflict of interest.

DATA AVAILABILITY STATEMENT

The data which are supporting the study's findings are available from the corresponding author upon reasonable request.

ORCID

Ulrich S. Schubert  <https://orcid.org/0000-0003-4978-4670>

REFERENCES

- [1] J. Lee, M. J. Cuddihy, N. A. Kotov, *Tissue Eng. B Rev.* **2008**, *14*, 61.
- [2] C. Jensen, Y. Teng, *Front. Mol. Biosci.* **2020**, *7*, 33.
- [3] E. C. Costa, A. F. Moreira, D. de Melo-Diogo, V. M. Gaspar, M. P. Carvalho, I. J. Correia, *Biotechnol. Adv.* **2016**, *34*, 1427.
- [4] S. A. Langhans, *Front. Pharmacol.* **2018**, *9*, 6.
- [5] M. Ravi, V. Paramesh, S. R. Kaviya, E. Anuradha, F. D. P. Solomon, *J. Cell. Physiol.* **2015**, *230*, 16.
- [6] C. Frantz, K. M. Stewart, V. M. Weaver, *J. Cell Sci.* **2010**, *123*, 4195.
- [7] A. S. Ahmed, U. K. Mandal, M. Taher, D. Susanti, J. M. Jaffri, *Pharm. Dev. Technol.* **2018**, *23*, 751.
- [8] A. M. Akimoto, E. Hasuike, H. Tada, K. Nagase, T. Okano, H. Kanazawa, R. Yoshida, *Anal. Sci.* **2016**, *32*, 1203.
- [9] C. Y. Ko, K. L. Ku, S. R. Yang, T. Y. Lin, S. Peng, Y. S. Peng, M. H. Cheng, I. M. Chu, *J. Tissue Eng. Regen. Med.* **2016**, *10*, E485.
- [10] N. Z. Zhou, K. Hu, Z. B. Guo, Q. Y. Zhang, J. S. Chen, T. Z. Zhang, N. Gu, *J. Nanosci. Nanotechnol.* **2018**, *18*, 5252.
- [11] K. Molyneaux, M. D. Wnek, S. E. L. Craig, J. Vincent, I. Rucker, G. E. Wnek, S. M. Brady-Kalnay, *J. Biomed. Mater. Res. B.* **2021**, *109*, 1744.
- [12] G. Bahcecioglu, B. Bilgen, N. Hasirci, V. Hasirci, *Biomaterials* **2019**, *218*, 119361.
- [13] S. Peng, S. R. Yang, C. Y. Ko, Y. S. Peng, I. M. Chu, *J. Biomed. Mater. Res. A* **2013**, *101*, 3311.
- [14] M. Bakhshpour, N. Idil, I. Percin, A. Denizli, *Appl. Sci.* **2019**, *9*, 553.
- [15] F. Behrendt, Y. Deng, D. Pretzel, S. Stumpf, N. Fritz, M. Gottschaldt, G. Pohnert, U. S. Schubert, *Mater. Horiz.* **2023**, *10*, 2412.
- [16] M. Razavi, Y. Qiao, A. S. Thakor, *J. Biomed. Mater. Res. A* **2019**, *107*, 2736.

- [17] C. J. Fan, Y. Ling, W. S. Deng, J. Q. Xue, P. Sun, D. A. Wang, *Biomed. Mater.* **2019**, *14*, 055006.
- [18] K. R. Hixon, T. Lu, S. A. Sell, *Acta Biomater.* **2017**, *62*, 29.
- [19] A. Katsen-Globa, I. Meiser, Y. A. Petrenko, R. V. Ivanov, V. I. Lozinsky, H. Zimmermann, A. Y. Petrenko, *J. Mater. Sci. Mater. Med.* **2014**, *25*, 857.
- [20] J. Kumari, A. Kumar, *Sci. Rep.* **2017**, *7*, 41551.
- [21] O. Senko, N. Stepanov, O. Maslova, E. Efremenko, *Sustainability* **2022**, *14*, 661.
- [22] N. E. Vrana, K. Matsumura, S. H. Hyon, L. M. Geever, J. E. Kennedy, J. G. Lyons, C. L. Higginbotham, P. A. Cahill, G. B. McGuinness, *J. Tissue Eng. Regen. Med.* **2012**, *6*, 280.
- [23] E. Jain, A. A. Karande, A. Kumar, *Biotechnol. Prog.* **2011**, *27*, 170.
- [24] J. Sarkar, A. Kumar, *Analyst* **2016**, *141*, 2553.
- [25] V. I. Lozinsky, F. M. Plieva, *Enzym. Microb. Technol.* **1998**, *23*, 227.
- [26] A. Golunova, J. Jaros, V. Jurtikova, I. Kotelnikov, J. Kotek, H. Hlidkova, L. Streit, A. Hampl, F. Rypacek, V. Proks, *Physiol. Res.* **2015**, *64*, S19.
- [27] N. Bolgen, Y. Yang, P. Korkusuz, E. Guzel, A. J. El Haj, E. Piskin, *Tissue Eng. A* **2008**, *14*, 1743.
- [28] N. Bolgen, Y. Yang, P. Korkusuz, E. Guzel, A. J. El Haj, E. Piskin, *J. Tissue Eng. Regen. Med.* **2011**, *5*, 770.
- [29] D. Singh, V. Nayak, A. Kumar, *Int. J. Biol. Sci.* **2010**, *6*, 371.
- [30] D. J. Borg, P. B. Welzel, M. Grimmer, J. Friedrichs, M. Weigelt, C. Wilhelm, M. Prewitz, A. Stissel, A. Hommel, T. Kurth, U. Freudenberg, E. Bonifacio, C. Werner, *Acta Biomater.* **2016**, *44*, 178.
- [31] Y. S. Hwang, C. Zhang, S. Varghese, *J. Mater. Chem.* **2010**, *20*, 345.
- [32] A. Singh, P. Tayalia, *J. Biomed. Mater. Res. A* **2020**, *108*, 365.
- [33] P. Jayal, P. Behera, R. Mullick, S. G. Ramachandra, S. Das, A. Kumar, A. Karande, *Biotechnol. Bioeng.* **2021**, *118*, 1286.
- [34] T. Watanabe, T. Sato, S. Yoshioka, T. Koshijima, M. Kuwahara, *Eur. J. Biochem.* **1992**, *209*, 651.
- [35] X. S. Chen, H. Gu, Z. L. Lyu, X. L. Liu, L. Wang, H. Chen, J. L. Brash, A. C. S. Appl, *Mater. Interfaces* **2018**, *10*, 1440.
- [36] S. B. Jiang, J. X. Wu, Y. J. Hang, Q. Liu, D. Li, H. Chen, J. L. Brash, *J. Mater. Chem. B* **2019**, *7*, 4017.
- [37] J. H. Lei, Y. Q. Yuan, Z. L. Lyu, M. M. Wang, Q. Liu, H. W. Wang, L. Yuan, H. Chen, A. C. S. Appl, *Mater. Interfaces* **2017**, *9*, 28209.
- [38] X. Y. Liang, A. Y. Zhang, W. Sun, J. Lei, X. L. Liu, Z. C. Tang, H. Chen, *Colloid Surf. B* **2022**, *212*, 112337.
- [39] Q. Liu, H. Xue, J. B. Gao, L. M. Cao, G. J. Chen, H. Chen, *Polym. Chem.* **2016**, *7*, 7287.
- [40] W. Sun, S. Jin, A. Y. Zhang, J. L. Huang, Y. P. Li, X. L. Liu, H. Chen, *J. Mater. Chem. B* **2020**, *8*, 9151.
- [41] F. Yu, S. Y. Cheng, J. H. Lei, Y. J. Hang, Q. Liu, H. W. Wang, L. Yuan, *J. Biomater. Sci. Polym. Ed.* **2020**, *31*, 1623.
- [42] A. Y. Zhang, W. Sun, X. Y. Liang, X. S. Chen, Y. P. Li, X. L. Liu, H. Chen, *Colloid Surf. B* **2021**, *201*, 111653.
- [43] T. Wloka, S. Czich, M. Kleinstaub, E. Moek, C. Weber, M. Gottschaldt, K. Liefeth, U. S. Schubert, *Eur. Polym. J.* **2020**, *122*, 109295.
- [44] X. Li, M. M. Bao, Y. Y. Weng, K. Yang, W. D. Zhang, G. J. Chen, *J. Mater. Chem. B* **2014**, *2*, 5569.
- [45] Procedure for EDC/NHS Crosslinking of Carboxylates with Primary Amines. https://www.thermofisher.com/document-connect/document-connect.html?url=https://assets.thermofisher.com/TFS-Assets%2FMSG%2Fmanuals%2FMAN0011309_NHS_SulfoNHS_UG.pdf. Accessed on April 6, 2023.
- [46] F. Behrendt, Z. Cseresnyés, R. Gerst, M. Gottschaldt, M. T. Figge, U. S. Schubert, *J. Biomed. Mater. Res. A* **2023**, *111*, 1734.
- [47] L. C. Bahlmann, A. E. G. Baker, C. Xue, S. Liu, M. Meier-Merziger, D. Karakas, L. K. Zhu, I. Co, S. Zhao, A. Chin, A. McGuigan, J. Kuruvilla, R. C. Laister, M. S. Shoichet, *Adv. Funct. Mater.* **2021**, *31*, 2008400.
- [48] O. B. Unluer, S. E. Diltemiz, M. G. Say, D. Hur, R. Say, A. Ersoz, *Int. J. Polym. Mater.* **2022**, *71*, 278.
- [49] S. B. Ki, D. Singh, S. C. Kim, T. W. Son, S. S. Han, *Biotechnol. Appl. Biochem.* **2013**, *60*, 589.
- [50] X. Y. Hu, Y. M. Wang, L. L. Zhang, M. Xu, *Int. J. Biol. Macromol.* **2019**, *126*, 221.
- [51] S. D. Gur, M. Bakhshpour, N. Bereli, A. Denizli, *J. Biomater. Sci. Polym. Ed.* **2021**, *32*, 1024.
- [52] G. Bayrak, I. Percin, A. K. Suloglu, A. Denizli, *Process Biochem.* **2021**, *110*, 100.
- [53] M. Bakhshpour, H. Yavuz, A. Denizli, *Artif. Cells Nanomed. Biotechnol.* **2018**, *46*, 946.
- [54] D. Berillo, L. Elowsson, H. Kirsebom, *Macromol. Biosci.* **2012**, *12*, 1090.
- [55] F. Ofkeli, D. Demir, N. Bolgen, *J. Appl. Polym. Sci.* **2021**, *138*, 50337.
- [56] N. Mehwish, Y. Chen, M. Zaeem, Y. Wang, B. H. Lee, H. Deng, *Int. J. Biol. Macromol.* **2022**, *214*, 617.
- [57] C. A. Schneider, W. S. Rasband, K. W. Eliceiri, *Nat. Methods* **2012**, *9*, 671.
- [58] J. Schindelin, I. Arganda-Carreras, E. Frise, V. Kaynig, M. Longair, T. Pietzsch, S. Preibisch, C. Rueden, S. Saalfeld, B. Schmid, J.-Y. Tinevez, D. J. White, V. Hartenstein, K. Eliceiri, P. Tomancak, A. Cardona, *Nat. Methods* **2012**, *9*, 676.
- [59] R. Gerst, Z. Cseresnyés, M. T. Figge, *Nat. Methods* **2023**, *20*, 168.
- [60] C. Stringer, T. Wang, M. Michaelos, M. Pachitariu, *Nat. Methods* **2021**, *18*, 100.

SUPPORTING INFORMATION

Additional supporting information can be found online in the Supporting Information section at the end of this article.

How to cite this article: F. Behrendt, D. Pretzel, Z. Cseresnyés, M. Kleinstaub, T. Wloka, L. Radosa, M. T. Figge, M. Gottschaldt, A. Brakhage, U. S. Schubert, *J. Polym. Sci.* **2023**, *61*(23), 3039. <https://doi.org/10.1002/pol.20230499>